

Repair of directionally solidified superalloy GTD-111 by laser-engineered net shaping

Leijun Li

Received: 9 February 2005 / Accepted: 23 December 2005 / Published online: 7 November 2006
© Springer Science+Business Media, LLC 2006

Abstract GTD-111 directionally solidified superalloy was repaired by the Nd:YAG laser based laser-engineered net shaping (LENS) process. Selection of process parameters are discussed against the formation of deposits and occurrence of defects. Formation of microfissures, porosity, lack of fusion, and stray crystals in the deposit zone was studied. It was identified that formation of stray crystals in the directionally solidified alloy could be due to two types of sources: the shape of the melt pool, and the existence of second-phase particles at the melt pool fusion boundary.

Introduction

GTD-111 is a γ' strengthened Ni-based superalloy that is widely used as the bucket material in land-based turbine systems. This alloy has a directionally solidified (DS) microstructure formed in the $\langle 100 \rangle$ crystallographic direction. This cast material was developed in the 1970's and introduced in the 1980's as an alternative to the buckets commonly made of IN738LC [1]. GTD-111 was an improvement made to GE's superalloy René 80. This material increased the creep rupture advantage over IN738LC by 20 °C. The material is proprietary and its nominal composition is listed in Table 1. Much of the strength of the material

comes from its high volume of gamma prime (γ') precipitation. The properties of this DS microstructure allow the alloy to withstand higher temperatures, improve creep rupture life, higher impact strength, greater thermal fatigue resistance, and better corrosion resistance.

The precipitation strengthening mechanisms and large directional dendritic microstructure that give GTD-111 the desirable high temperature properties also make it difficult to repair. All current repair specifications require material to be added to the bucket to have similar properties found in the base material. The repaired material must withstand extreme temperatures, vibration and thermal stresses, impact damage from foreign objects, and tip rub [2]. The method of application must be able to achieve appropriate cohesion of the filler material to the original base material without sacrificing the integrity of the base structure.

Of the repair methods available, the LENS (Laser Engineered Net Shaping) system was selected for its potential for turbine bucket repair. LENS is a new rapid prototyping technology that has been used in industry for repairs, fabrication of new materials, and development of tooling. Excellent examples of research into produce innovative metal matrix composites can be found in works by Liu and DuPont [3, 4]. LENS's ability to control material deposition and minimize heat input makes it a desirable method for turbine bucket repair. This paper reports a study that investigated the effect of LENS process parameters on the formation of René 80 deposition on a GTD-111 substrate. The resultant deposits will be characterized, and the defects encountered in the LENS process will be discussed.

L. Li (✉)
Department of Mechanical & Aerospace Engineering,
Utah State University, Logan, UT 84322-4130, USA
e-mail: leijun.li@usu.edu

Table 1 Chemical composition (in wt%) of test alloys

Element	GTD-111	PARXAIR Ni138 (René-80)
Al	2.8–3.2	2.80
B	0.01–0.02	0.01
C	0.08–0.12	0.18
Co	9.0–10.0	9.66
Cr	13.7–14.3	14.09
Cu	–	0.05
Fe	–	0.05
Hf	0.02–0.08	0.10
Mg	–	0.001
Mn	–	0.10
Mo	1.3–1.7	4.03
N	–	0.0049
Nb	–	0.05
O	–	0.01
P	–	0.005
S	–	0.0017
Se	–	0.005
Si	–	0.10
Ta	2.5–3.1	0.10
Ti	4.8–5.1	4.83
V	–	0.05
W	3.5–4.1	3.91
Zr	0.02–0.08	0.06
Ni	Balance	Balance

Experimental procedures

The LENS system employs a 500W Nd:YAG laser to heat a stream of powder at a precise location while in an argon environment. It differs from other rapid prototyping methods in that it takes the material in powder form and creates a final, usable product in one stage. It has a four-port powder feeder system that injects powder via pressurized argon into the laser beam which is focused near the surface of the substrate. The laser melts the powder and achieves a metallurgical bond of the powder and the substrate at the point of convergence of powder flow.

The René 80 powder was chosen as the filler materials, because it is the only commercially available powder alloy with almost the same composition of GTD-111. The chemical composition for the filler powder is shown in Table 1. The test coupons were cut perpendicularly to the bucket axis (the $\langle 100 \rangle$ direction) from a GTD-111 turbine bucket that had not experienced service, had not received a surface coating, and was in an annealed state. The material was cut using wire EDM and a liquid-cooled sectioning saw to minimize heat damage to the microstructure. The deposition surface was prepared by sanding with #600 sand paper and cleaned with acetone. The LENS deposit was placed on the (100) plane of the GTD-111 test coupon. The deposit zone was designed to be a

6.35×9.65 mm rectangle and approximately six passes high (about 0.25 mm thick for each pass). Height and shape of each deposit sample were varied as a result of adjustment in energy input and powder feed rate.

Deposition parameters, including the hatch line distance, laser scan rate, powder feed rate, and laser power levels, were screened for a stable deposition process. The parameters that were varied during the actual experiments are laser scan speed and the laser power level. The oxygen level in the glove box was 5–10 ppm. The laser energy input was taken from the amperage indicator on the 500W Nd:YAG laser. No pre-heat or post-deposition heat treatment of the deposited samples was employed. The sequence for a deposition layer consisted of a pass that outlines the shape of the deposit zone. The internal of the outlined deposit zone was then filled with passes. A test coupon is shown in Fig. 1 with the deposit areas each produced with a different combination of process parameters. The deposited coupons were cut for characterization with wire EDM. All samples were mounted and prepared according to standard metallographic procedures. The Marble's reagent was used for etching the samples. The samples were analyzed using a ZEISS Axiovert 100A metallurgical microscope with a PAX-cam FW-24 camera and PAX-It imaging software.

Results and discussion

Characterization of the deposits

Strong metallurgical bonding has been achieved between the deposit zone and the substrate. An example of deposit zone in the as-polished condition



Fig. 1 A GTD-111 test coupon showing the deposit areas

(Fig. 2) exhibits no boundary between the deposit and the substrate. The lower portion of the photomicrograph shows the substrate with bigger carbide particles; the upper portion of the photomicrograph shows the deposit layer with finer carbide particles.

After etching, directional dendritic structure in the substrate GTD-111 was revealed (Fig. 3). The refined dendritic structure in the René 80 deposit zone shows an epitaxial growth parallel with the GTD-111 substrate dendritic direction. The epitaxial growth also verifies the nature of bonding at the interface to be metallurgical. With proper deposition parameters, it was able to produce continued directional growth in the deposit zone over several layers. Figure 4 shows such an example, in which the directional dendritic growth has continued for four layers in the deposit. The epitaxial growth occurred not only at the interface between the first layer deposit and the substrate GTD-111, it also occurred at the interfaces between the subsequent layers. In Fig. 5, such continuous growth is clearly visible. The bottom layer shows a cellular dendritic structure and the top layer shows a columnar dendritic structure. Therefore, as subsequent layers were deposited, the solidification substructure seems to have changed from cellular to cellular dendritic and columnar dendritic.

The change in solidification substructure can be explained using the welding solidification theory [5]. The ratio of the temperature gradient, G , to the growth rate, R , in G/R , governs the mode of solidification. A lower G/R ratio favors dendritic substructure; a higher G/R favors cellular substructure. In the deposits, upper

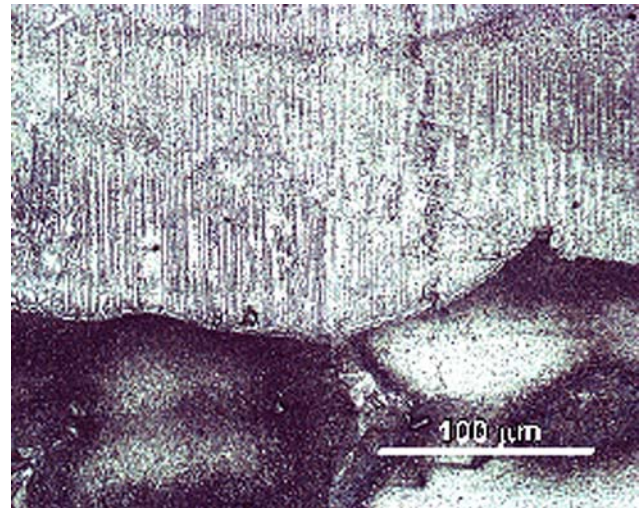


Fig. 3 Microstructure near the deposit–substrate interface showing epitaxial directional growth of dendrites in the deposit zone

layers have a lower temperature gradient G compared with the first layer, therefore, a transition occurred from cellular to a cellular dendritic substructure in multi-layered deposits. Compared with the dendritic size of the GTD-111 base metal, the primary dendrite size in the deposit zone is approximately 100 times smaller. The fine dendrite arm spacing in the deposit can be approximately described by the relation $\lambda = a(T_s/GR)^n$ where a is constant and T_s is the non-equilibrium temperature range of solidification and n is the exponent close to 0.5 [6]. Laser deposition process has a characteristic high GR value. Therefore, the

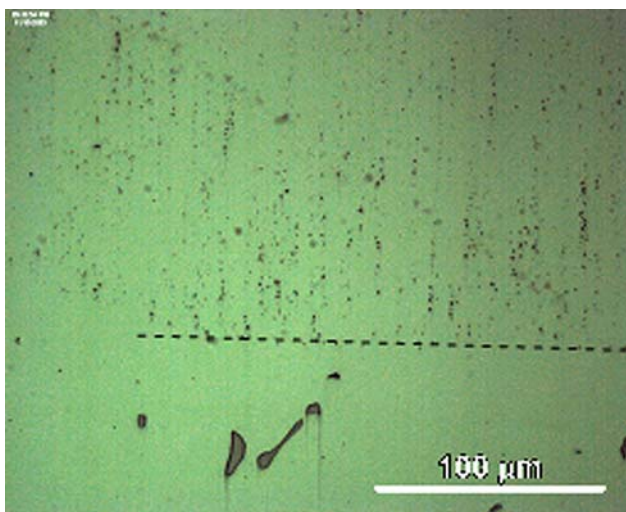


Fig. 2 Microstructure of an as-polished sample showing different sized carbide particles across the deposit–substrate interface, which is indicated by the dashed-line

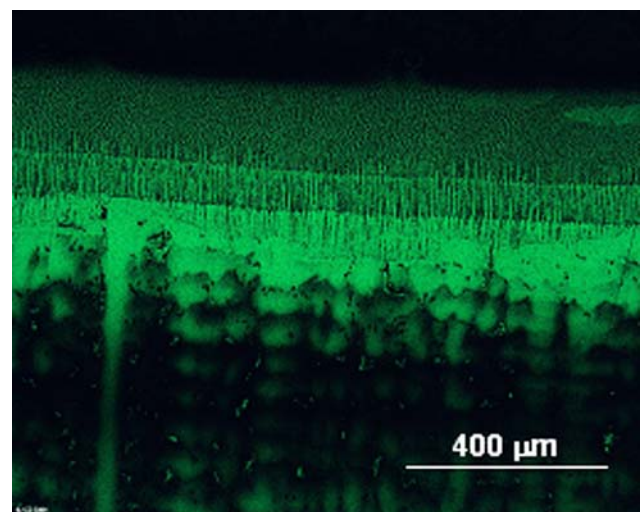


Fig. 4 Growth of multilayer directional dendritic structure in the deposit. The lower part of the photomicrograph is the GTD-111 substrate

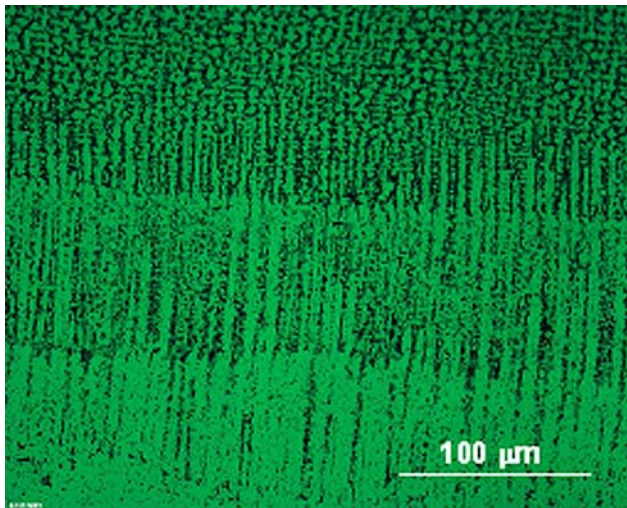


Fig. 5 Higher magnification of Fig. 4. The first layer appears to be of cellular dendritic morphology; subsequent layers become progressively more columnar dendritic

dendrite arm spacing has decreased significantly from the original cast alloy.

Defects in the deposit

Several forms of defects were observed in the deposit zone. The most common defect is the porosity, which can take the form of spherical hole with a diameter of approximately 80 μm (Fig. 6), or take the form of cavity with irregular shapes about 400 μm in size (Fig. 7). The formation of spherical porosity must have occurred before and/or during the solidification of the molten pool, because formation of a spherical gas bubble requires a surrounding liquid. Since the glove

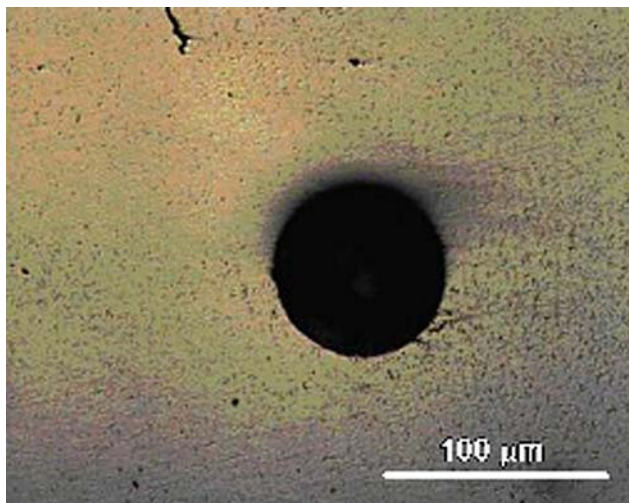


Fig. 6 A spherical porosity in the deposit

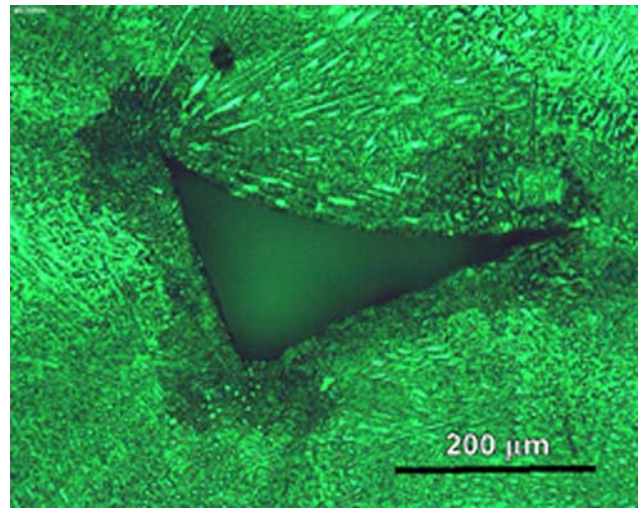


Fig. 7 Irregular shaped cavity in the deposit due to lack of fusion of feeding powder particles

box for the LENS process had a high vacuum back-filled with argon, the origins of the gases should be from the filler powder or the base metal. By baking the filler powder immediately before depositing, the tendency for spherical porosity formation has been significantly decreased. Another way to control the formation of spherical porosity is by increasing the heat input for laser deposition. A decreased solidification rate increases the chances for gaseous phase to migrate to the atmosphere before the molten pool solidifies.

The irregular shaped cavity shown in Fig. 7 is believed to be due to the lack of fusion between filler powder particles. To prevent this type of porosity from happening, it requires a coordinated adjustment of powder feed rate and laser power level. Complete fusion of feeding powder particles can be achieved and this type of cavity can be eliminated through optimized powder feeding rate and laser energy.

Another related lack of fusion defect occurred at the first-layer deposit and the GTD-111 substrate interface (Fig. 8). This defect can be avoided by adjusting the laser power and powder feed rate, in addition to adjusting the hatch line distance (the amount of overlap between laser deposition passes).

The microfissure is another form of defects observed in the deposit. An example of microfissure is shown in Fig. 9. The typical microfissures are about 200 μm long, and tend to form along the grain boundaries. Because of this association of microfissuring with the grain boundary, the tendency for fissuring seems to increase with the formation of “stray” grains, i.e., grains growing along directions other than the $\langle 100 \rangle$ direction of the

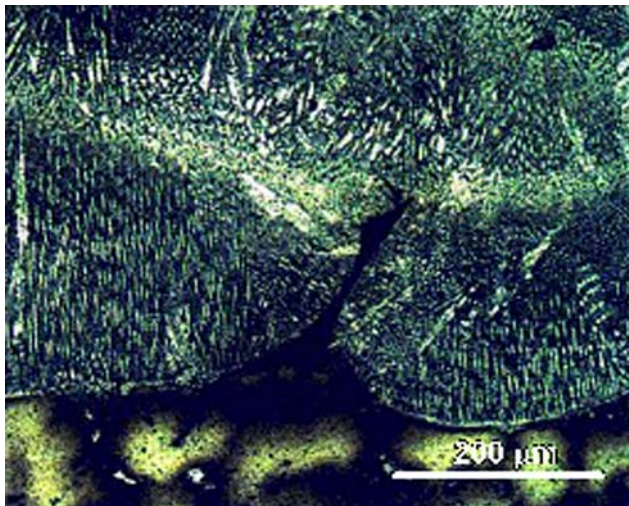


Fig. 8 Lack of fusion at the deposit and substrate interface

substrate. Since the stray grains tend to form more frequently in the third layer and subsequent layers, these microfissures are more frequently observed in the upper layers of the deposit. However, microfissures can also occur, although much less frequently, at the lower layers of the deposit. Figure 10 shows an example of fissuring in the first layer. This fissure is associated with a grain boundary of the base metal GTD-111.

Processing parameters were found to affect the microfissure tendency. Figure 11 shows the effect of laser power and scan speed on the number of fissures in the deposited zone. The number of fissures was determined metallographically at $175\times$ magnification on the entire cross-section of a mounted sample. Other conditions kept the same, increasing the laser power has the effect of increasing microfissure tendency. While

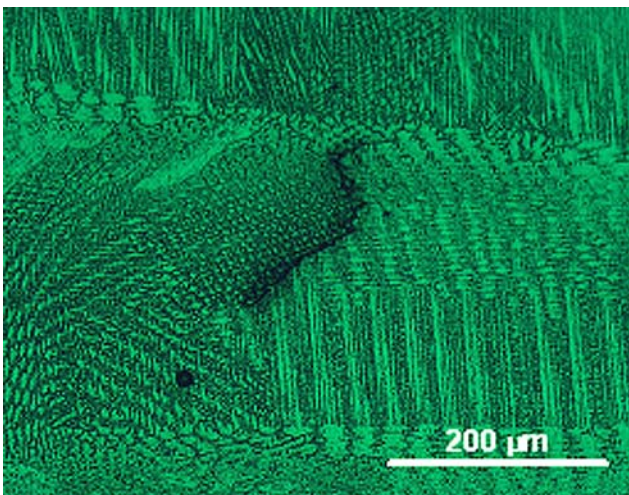


Fig. 9 A microfissure formed along a "stray" grain boundary

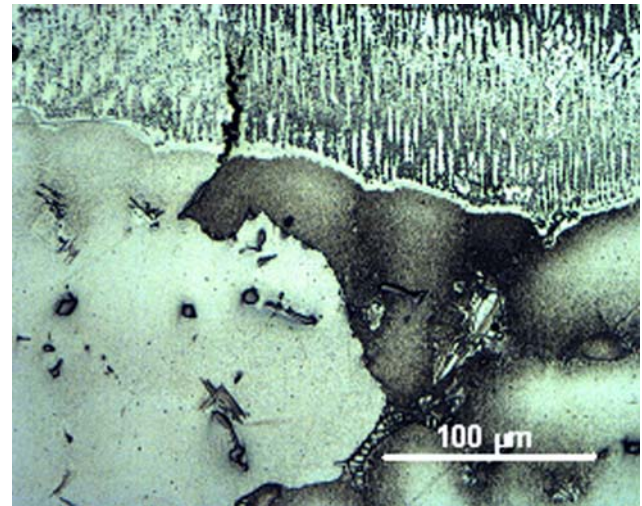


Fig. 10 A microfissure formed as an extension of the grain boundary in the base metal and extends along the inter-dendritic interface in the deposit

increasing the scan speed has the effect of decreasing the microfissure tendency. The mechanism through which the process parameters affect the fissuring tendency involves creation of thermal stresses and creation of unfavorable microstructure and thus properties. The microstructure evidence seems to indicate the role of stray grains in enhancing microfissuring. The formation of stray grains, as discussed later, is also dependent on the thermal conditions of the deposition, and therefore directly related with the laser processing parameters.

The characteristics of the microfissures seem to belong to those of hot cracking commonly seen in superalloy weld metals. When the ductility of the alloy is not enough to withstand the thermal stresses, fissuring may occur. Additionally, the lower melting

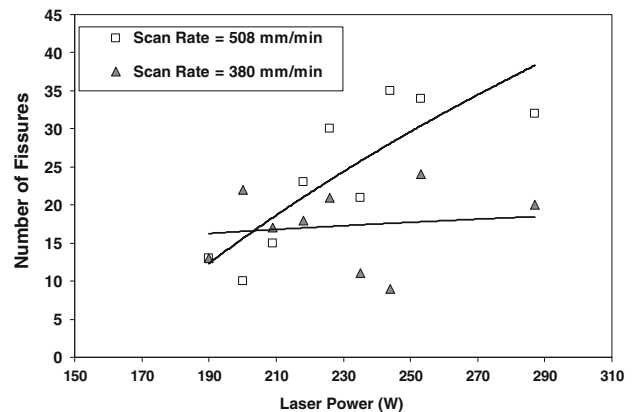


Fig. 11 Effects of laser current and scan rate on number of fissures

point components such as boron and silicon were rejected into the liquid in front of solid–liquid surface and result in low melting phase forming at grain boundaries and inter-dendritic region in last solidification areas. This effect decreases the ductility of the grain boundaries. An effective method to prevent the strain related hot cracking is to apply sufficient preheat. In addition, a properly specified post weld heat treatment (PWHT) will relieve the residual stresses and avoid delayed cracking.

Stray grains formation

It is desirable to preserve the direction of dendrite in the base GTD-111 alloy in the deposits. However, the mis-orientated grains known as stray grains were observed in the deposits. Such stray grains will form large-angle grain boundaries with adjacent grains, which impair the mechanical properties of deposit and lead to microfissuring. Stray grains observed in the deposits can be classified into two types: (1) Type 1—stray grains caused by change of heat transfer condition (melt pool shape), growing at 90° relative to preferred < 100 > direction, (2) Type 2—stray grains caused by local disruptions due to second-phase particles, growing at random directions.

Figure 12 shows a deposit zone containing Type 1 stray grains. The stray grains tend to form at the sides of the weld pool where there is a change of curvature of the fusion line (as indicated by A in Fig. 12). The shape of molten pool seems to have a direct influence on the formation of stray crystals. Similar observations had been made in numerous studies by others, e.g.,

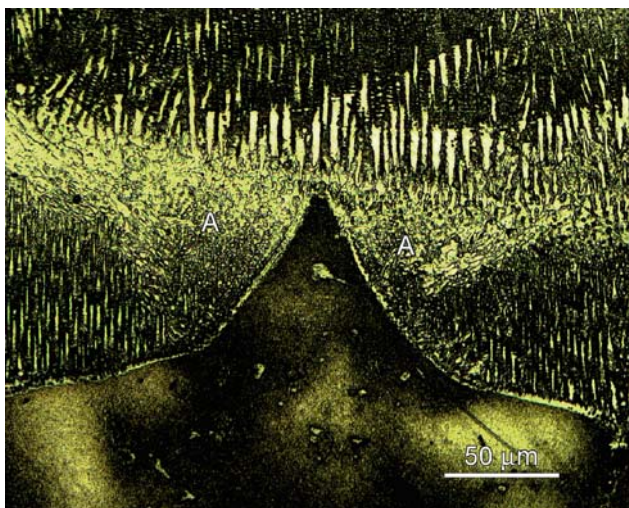


Fig. 12 A deposit zone with stray grains (indicated by A) formed along directions 90° from the substrate < 100 > dendritic direction

in [7]. The weld solidification theory has a generally accepted explanation for this observation. It is believed that the direction of crystal growth in the molten pool depends on two main factors: the preferred crystallographic orientation of the growing crystal, and direction of heat flux [6]. If the direction of heat dissipation is opposite to the preferred growth direction for a dendrite (< 100 > for cubic crystals), a higher growth rate allows the dendrite to dominate the solid/liquid morphology and out grow competing dendrites.

From an experimentally measured weld pool geometry, Liu and DuPont [8] developed a mathematical model to predict the crystal growth and microstructure development in laser surface-melted superalloy single crystals. The weld pool was effectively approximated by a double-ellipsoid, with α being the angle between the substrate surface and the tangent of the weld fusion line in the transverse cross-section (Fig. 13). Liu and DuPont calculated and verified experimentally that if α angle is less than 45°, no stray crystals will form in the solidified deposit. Measurement results from this study also confirmed the 45° seems to be the critical angle for stray grain formation for directionally solidified alloy (Fig. 14). The angle β as defined in Fig. 13 is the angle between the normal vector to the fusion line and the z axis. The relation between β and α angles are as follows: for a given weld pool, angle β is always less than angle α , with the maximum β equal to α . This can be mathematically verified from the equation that describes the ellipsoid in the y–z plane (Fig. 13):

$$\frac{y^2}{B^2} + \frac{(z - D)^2}{(h + D)^2} = 1$$

The angle β equals to $\arctan(\frac{dz}{dy})$, where

$$\frac{dz}{dy} = -\frac{y}{B^2} \frac{(h + D)}{\sqrt{1 - \frac{y^2}{B^2}}}$$

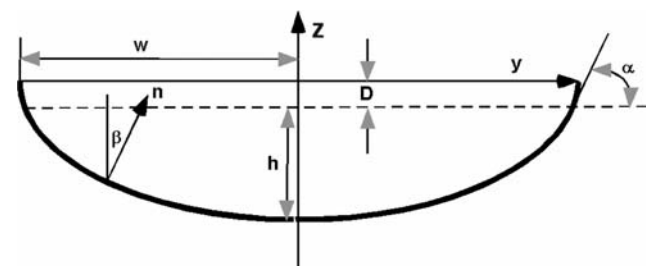


Fig. 13 Schematic of cross-section of deposit represented as part of an elliptical curve. α refers to the angle between the fusion line and the top surface, β refers to the angle between the normal of fusion line curve and the vertical axis (< 100 > growth direction of the substrate material)

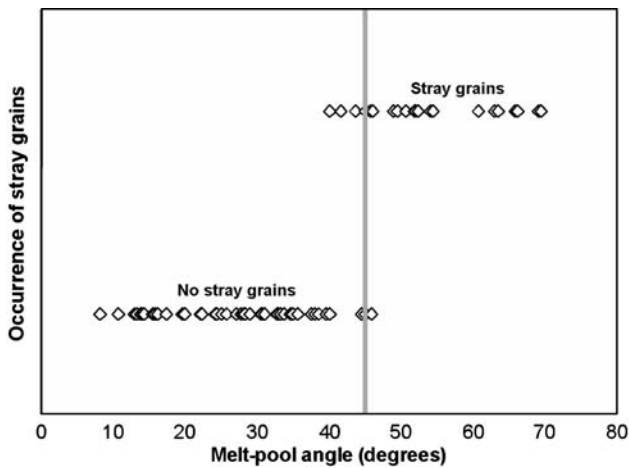


Fig. 14 Relationship between the β angle and the occurrence of stray grains in the deposit. 45° seems to be the critical β angle for formation of stray grains

It follows that for any y value less than w ($1/2$ of the width of the melt pool B), β is always less than α . The occurrence of Type 1 stray grains in this study can be characterized by the β angle. If β is smaller than the critical value of 45° , directional solidification along z direction will occur, otherwise stray crystals will form at 90° to z axis.

Type 2 stray grains in the laser processed directionally solidified superalloy is associated with second-phase particles in the substrate alloy. A typical example is shown in Fig. 15. Compared with Type 1, Type 2 stray grains form at a localized disruption to the otherwise smooth fusion boundary. Although the β angle for the

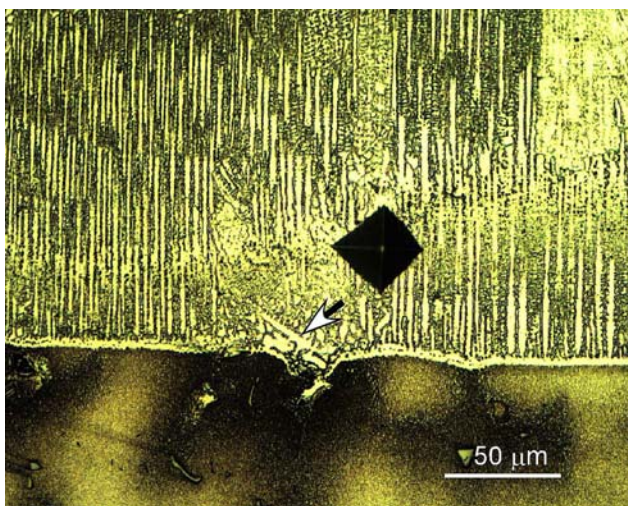


Fig. 15 A stray grain (indicated by the arrow) grown from a cusp associated with a second-phase particle on a grain boundary in the GDT-111 substrate

fusion boundary does not satisfy the condition for stray grain growth, a small cusp along the fusion boundary formed due to dissolution and liquation of the second-phase particle promotes formation of stray grains. The non-equilibrium particle dissolution produces a suppression of melting points around the dissolving particle [9]. This suppression of melting points is believed to result in the formation of cusps along the fusion boundary of the weld pool. Since Type 2 stray grains are associated with dispersed second-phase particles, they should not form if second-phase particles are not present near the fusion boundary. An experimental verification was conducted by continued polishing and tracking the appearance of stray grains. Microhardness indentations were made near the stray gains for tracking the field of views. The depth of sample surface moved was calculated using the fixed 136° included angle for the diamond indenter and by measuring the hardness indentation diameter before and after polishing. An example is shown in Fig. 16, which shows the same field of view as shown in Fig. 15 but after a 5-micron thick layer had been removed. There are no stray grains, nor second-phase particles at the previous stray grain site.

The mechanisms of stray grain formation have been recently studied by some researchers. Park et al. [10] believed that stray grain formation was sensitive to crystallographic orientation of growing dendrites as well as processing conditions. The processing conditions influence the constitutional super-cooling at the solidification front. Sajjadi et al. [11] postulated that the misorientations may have resulted from the thermo-mechanical stresses formed during the γ' precipitation at temperatures slightly below the solidus temperature

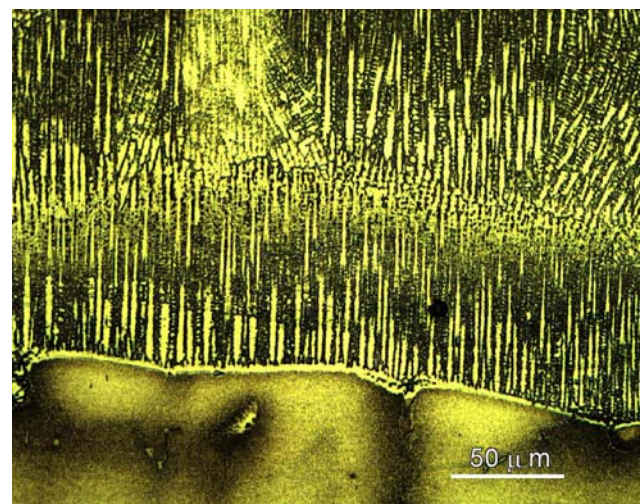


Fig. 16 Same location as shown in Fig. 15, after removing about $5 \mu\text{m}$ by polishing. No stray grain is found

of the alloy. Gaumann et al. [12] proposed that any unmelted powder particles in the deposit may have provided the new nucleation sites for the stray grains. Based on the results of this study, we believe Park et al's and Liu and DuPont's proposed mechanisms are more appropriate for explaining stray grain formation in laser deposited directionally solidified superalloys.

Conclusions

René 80 has been successfully deposited on GTD-111 superalloy substrate by the laser-engineered net shaping process. Microstructural analysis shows a metallurgical bonding has been achieved between the deposit and the substrate. With optimized process parameters, a multi-layered, directionally solidified microstructure can be achieved in the laser deposit. The resultant microstructure was considerably smaller than the substrate. Defects in the deposits, including porosity, microfissuring, and formation of stray grains, were observed and the causes and prevention methods were discussed. Two types of stray grains were identified in the deposits. The formation of Type 1 stray grains is believed to be dependent on the overall weld pool shape as determined by the process parameters. The

formation of Type 2 stray grains is believed to be associated with the second-phase particles in the substrate that are near the fusion boundary.

Acknowledgements The author would like to thank Ms. Anne Koleman of General Electric for providing the GTD-111 bucket test material and research assistants Mr. Michael Harrison and Mr. Tian Tang for helping with the experiments.

References

1. Daleo JA, Wilson JR (1998) *J Eng Gas Turbine Power* 120:375
2. Sims CT, Stoloff NS, Hagel WC (1987) *Superalloy II*. John Wiley & Sons, New York, p 98
3. Liu W, DuPont JN (2003) *Scripta Mat* 48:1337
4. Liu W, DuPont JN (2003) *Met Trans A* 34A:1337
5. Messler RW Jr (1999) *Principles of welding*. John Wiley & Sons, p 428
6. Kurz W, Fisher DJ (1989) *Fundamentals of solidification*, 3rd edn. Trans Tech Publications
7. David SA, Vitek JM, Babu SS, Boatner LA, Reed RW (1997) *Sci Technol Welding Joining* 2(2):79–88
8. Liu W, DuPont JN (2004) *Acta Mater* 52:4833
9. Li L, Messler RW Jr (2002) *Mat Met Trans A* 33A(7):2031
10. Park JW et al (2003) *J Appl Phys*
11. Sajjadi SA et al (2002) *Mater Sci Eng A* 325, p 484
12. Gaumann M, Bezencon C, Canalis P, Kurz W (2001). *Acta Mater* 49:1051